A Diagnostic Model for the Combustion of Seed Oils in Diesel Engines

H.C. Watson, S. Kumar, E. Milkins and J. Edsell,
University of Melbourne

ABSTRACT

A phenomenological model for the open chamber diesel engine combustion is presented which is modular in concept. The modules for fuel injection, jet penetration and droplet formation have been calibrated outside the engine with the aid of a high pressure, fixed volume chamber. In a diagnostic mode of operation the chemical component of the ignition delay can be estimated.

In a predictive mode of operation the model is used to closely estimate an engines' pressure diagrams over a wide range of speed and load conditions.

INTRODUCTION

Combustion problems from fuelling the open chamber diesel engine with the oils of plants such as the sunflower have been documented by many researchers (1,2). The major problems, usually occurring after some tens of hours of operation can be summarised as injector fouling, ring sticking and bearing damage. There is evidence that by changing the physical and chemical composition of the plant oil through, for example, esterification more durable engine operation can be achieved. It is not clear whether the enhanced performance is the result of the changed physical properties such as viscosity, surface tension etc. or the change in the bond structure of the complex acids which form the major constituents of the fuel.

OBJECT

The object was to provide an understanding of the relative importance of the changed fuel properties between automotive distillate and some plant oils and their constituents in their influence on the diesel engine combustion process. This object was to be achieved through the calibration of a phenomenological model which could then be used to carry out sensitivity analyses to fuel property and some engine design changes.

OUTLINE OF PAPER

In this paper the model for the diesel engine combustion process is summarised. The experimental techniques developed to calibrate the model are described in outline and the preliminary results of the application of the model presented.

THE MODEL

Major Features

The model has two modes of operation:

1. Diagnostic in which it is employed to determine coefficients for the fuel-air reaction.
2. Predictive in which it is employed to provide estimates of the sensitivity of the combustion process to changes in fuel properties.

As the model is of modular design, it is only the last of the modules which are altered to perform the second role just identified. The modules perform the following tasks:

1. Description of the injector nozzle delivery pressure, essential to describe the fuel flow rate into the combustion chamber.
2. Calculation of the droplet size distribution and its spatial and temporal distribution within the fuel jet as influenced by injection pressure, surrounding conditions and
3. The rate of droplet evaporation including the tendency for fuel droplets to reach critical conditions.
4. Entrainment of air into the starting jet and the ensuing wall jet when impingement on the wall of the piston bowl occurs.
5. The rate of oxidation of the prepared fuel-air mixture controlled by the overall reaction kinetic processes.
6. Heat transfer to the cylinder walls which is based on the premise that the laminar sub-layer has dominating influence on the heat transport process.

Each of the modules are now described.

Fuel Injection

Space limitations within the engine precluded the measurement of the injector 'tip' or sac pressure immediately upstream of the 3 injector orifices. This is needed to calculate the fuel

injection rate. We were forced to measure the line pressure about 150 mm from the fuel injector tip. Observation that the line pressure was influenced by the test chamber pressure during the experiments (described later) to measure the fuel jet properties led to the conclusion that prediction of the injector sac pressure was necessary.

As had been shown by Wylie et al (3) it is possible to describe mathematically the flow and pressure throughout the fuel delivery line and injector system. However, the time delays associated with the acoustic nature of wave propagation require solution by numerical methods involving significant computer time viz. the method of characteristics.

For simplicity we have described injector sac pressure P_s by way of a correlation analysis of experimental data. The fuel injector was removed from the engine and P_s measured with a piezo-electric transducer through an auxilliary hole drilled into the injector nozzle.

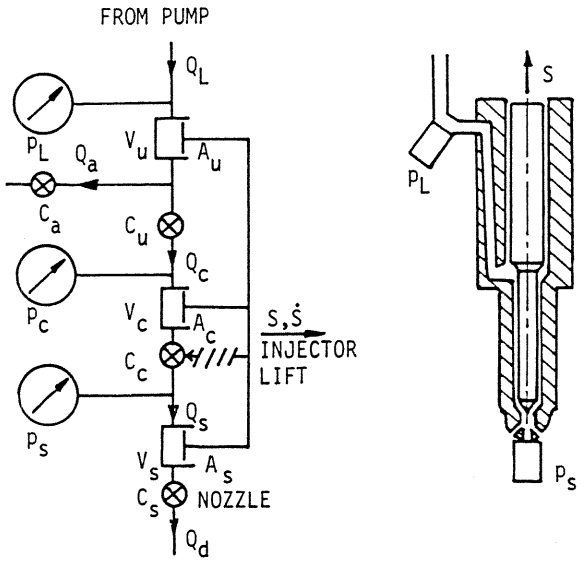

Fig. 1 Schematic of fuel injector and location variables used in equation 1-6

In the schematic diagram of the injector shown in Fig. 1 the inflow pressure P_L is the measured line pressure for each engine operating condition, and also measured in the correlation experiment. The injector needle lift S is also always measured. The flow Q through each of the chamber volumes V is restricted by resistances (area x flow coefficient) C. As the needle lift increases at a rate S the chamber volumes will increase at a rate AS where A is their cross sectional area. If the compressibility of the fuel is k, then

$$\frac{dP_L}{dt} = \frac{k}{V_u + A_u S}(Q_L - Q_c - Q_a - A_u \dot{S}) \quad (1)$$

$$\frac{dP_c}{dt} = \frac{k}{V_c + A_c S}(Q_c - Q_s - A_c \dot{S}) \quad (2)$$

$$\text{and} \quad \frac{dP_s}{dt} = \frac{k}{V_s + A_s S}(Q_s - Q_d - A_s \dot{S}) \quad (3)$$

where the subscripts u, c and s denote the upper nozzle, chamber volume upstream of the needle seat and the sac volume. Q_d is the delivered fuel injection rate.

Now the orifice flows are given by

$$Q_c = C_u \{2(P_c - P_L)/\rho_{f_u}\}^{1/2} \quad (4)$$

$$Q_s = C_c \{2(P_s - P_c)/\rho_{f_c}\}^{1/2} \quad (5)$$

$$Q_d = C_s \{2(P - P_s)/\rho_{f_s}\}^{1/2} \quad (6)$$

where ρ_f is the fuel density and P is the cylinder pressure.

The above equations were rearranged to describe P_s in terms of P_L and its derivative, and the needle lift S and its derivative $\dot{S}$. Since many of the flow areas used in the equation are difficult to measure, the coefficients and the time dependence were obtained at the 9 operating conditions as described later in the firing experiments. Because the pressure transducer was connected to the sac volume through the drilling as indicated in Fig. 1, operation was restricted to injection into atmospheric surroundings.

Thus P_s was correlated with variables such that

$$P_s = f(P_L, \frac{dP_L}{dt}, P_L(t), S, \dot{S}, N) \quad (7)$$

where $P_L(t)$ were the pressures at each of 3 preceeding 1^o CA intervals and N was the fuel injector cam speed.

The function obtained (4) was able to explain P_s with a correlation coefficient of 0.99 and a maximum predictive error of 14 atmospheres (10 % error) over the entire speed and load range.

Spray Development and Air Entrainment

The spray development is described by means of a one dimensional model in which the fuel jet is divided into zones (5,6) .

It is assumed that there is no mixing between zones even though the fuel droplets in the first injected zone may be overtaken by later injected fuel droplets, since the penetrations of each spray zone is described by the equation

$$s_p = C_1 \{\frac{\dot{m}}{\rho}\}^{1/4} t^{1/2} \quad (8)$$

where $\dot{m}$ is the flow rate of the fuel through the injector nozzle at time t into a medium of density ρ

The coefficient C_1 was calibrated using high speed photography in the high pressure combustion chamber described in Appendix A. For automotive diesel oil C_1=1.081.

The same experiment was employed to determine optically the semi-spray angle α. It follows from geometrical considerations that prior to impingement on the combustion chamber walls the entrainment of air for any zone V_{a_i} at time t_j will be

$$V_{a_i} = \frac{\pi}{3} \tan^2(\alpha) \{S_p(t_j)^3 - S_p(t_{j-1})^3\} \quad (9)$$

As described in Appendix B, the radial growth of the wall jet is governed by mass conservation, and is given by

$$r_w = C_2/(u_0 \; D \; t_w H^{0.2})^{2.2} \quad (10)$$

where u_0 is the fuel velocity at injection, D is the injector nozzle diameter, t_w is the time from commencement of wall jet and H is the distance from the injector to the wall on which the spray impinges. The constant C_2 was calculated to be 2.683.

Also in Appendix B it is shown that the wall jet entrainment can be expressed as

$$\frac{\dot{m}_w}{(\dot{m}_i)_o} = 9.386 \left(\frac{r_w}{D}\right) \left(\frac{r_w}{H}\right)^{-0.3} \quad (11)$$

where $\dot{m}_w$ is the mass flux at r_w and $(\dot{m}_i)_o$ is the mass flux at nozzle exit.

Droplet Evaporation

The module describing the evaporation of liquid fuel and the mixing of the fuel vapor with the entrained air in each zone embodies the concept of discrete droplet sizes which, nonetheless, conform to the function proposed by Kamimoto and Matsuoka (7), which is

$$\frac{dm_i}{m_i} = C_3 \; Y_i^{5.0} \exp(-5Y_i) \; dY_i \quad (12)$$

where m_i is the mass of liquid fuel in each zone and the dimensionless droplet size Y_i is given by

$$Y_i = D_d/\bar{D}_s \quad (13)$$

$\bar{D}_s$ being the Sauter mean diameter.

Hiroyasu et al (8) have indicated that the Sauter mean diameter can be expressed as injector to combustion chamber pressure difference Δp, injection rate at the time of the zone was injected $(m_i)_o$ and the density ρ as follows:

$$\bar{D}_s = C_4 \; (\Delta p)^{-0.135} \; (\rho)^{0.121} \; (B)^{0.131} \quad (14)$$

The coefficient C_3 and C_4 can be determined in the high pressure combustion bomb using a Laser droplet sizer as described in Appendix A.

The distribution of droplets described by equation 12, 13 and 14 is approximated to one having seven discrete initial sizes, which subsequently reduce by evaporation. In each jet zone i droplet survival is controlled by the following processes:

1. Evaporation

$$\frac{dM_d}{dt} = 2\pi \; D_d \; \frac{D_v}{(R_f T)} \; Sh \; (P_{fvs} - P_{fv}) \quad (15)$$

where M_d is the droplet mass (of a given size in zone i)
D_d is the droplet diameter
D_v is the diffusion coefficient
R_f is the fuel vapor gas constant
T is the zone temperature
Sh is the Sherwood number
P_{fv} is the partial pressure of the fuel vapor in the zone distant from the droplet
and P_{fvs} is the partial pressure of the fuel vapor at the droplets' surface.

The derivation of equation 15 may be found in reference (9), and is able to accommodate temperature and pressure conditions close to the critical point of the fuel.

2. Energy Conservation

$$M_d C_{p_f} \frac{dT_d}{dt} = \pi D_d \lambda Nu \; (T - T_d) \; \frac{\psi}{(e^{\psi} - 1)} + h_{fg} \frac{dM_d}{dt} \quad (16)$$

$$\text{where } \psi = \frac{-C_{p_{fv}} \frac{dM_d}{dt}}{(\pi D_d \lambda \; Nu)} \quad (17)$$

C_{p_f}, $C_{p_{fv}}$ are the specific heats of the fuel liquid and vapor (at mean film conditions).
T_d is the droplet temperature. λ is the thermal conductivity at mean film conditions. h_{fg} is the evaporation enthalpy and Nu is the Nusselt number.

3. Momentum

$$M_d \frac{dv_d}{dt} = -C_d \frac{\pi}{4} D_d^2 \rho \frac{v_d^2}{2} \quad (18)$$

where v_d is the droplet velocity
C_d its drag coefficient
ρ is the zone density

Fuel Oxidation

The fuel combustion module is based on the assumption that the vapor-air mixture in any zone burns according to:

$$\tau \frac{dM_b}{dt} + M_b = M_{fv} \quad (19)$$

where τ is a relaxation parameter
M_b is the mass of burnt fuel
M_{fv} is the mass of vaporised fuel

This first-order relaxation equation replaces the several equations describing the chemical kinetic and mixing processes as employed by Zeleznik (10). τ can be specified in many ways including an Arrhenius function as chosen here in the form

$$\tau = \frac{1}{K \; (1-b) \; (1 - \phi \; b)} \exp\left(\frac{E}{R \; T}\right) \quad (20)$$

where K is a constant
E is the activation energy of the overall reaction
ϕ is the fuel based equivalence ratio
and b is the burnt mass fraction.

This implies that in the multi-step oxidation of the fuel there exists a rate limiting reaction which dominates the overall reaction process.

At the beginning of simulation, values of K and E have been taken from a recent work (11). However a diagnostic mode of operation of the model has been created in which K and E can be determined as described shortly.

Heat Transfer

It is well known that the role of heat transfer in engine cycle simulation is such that it has relatively little influence on the prediction of peak cylinder pressure, although it may be more influential on the work per engine cycle.

In our early research into engine heat transfer (12) we had demonstrated that the prediction of the heat transfer in the laminar sublayer had a dominant influence on the heat loss from the in-cylinder charge. We have incorporated this concept into the present model since it explains the phenomenon of heat transfer in motored engines much better than models based on pipe flow analogies.

The following assumptions are made in the present model.

(i) All viscous dissipation effects are negligible.

(ii) The working gas is an ideal gas and the thermal conductivity of the gas is proportional to the absolute temperature.

(iii) Pressure is uniform at any instant of time but changes with time.

(iv) Fluid movements along the wall in the boundary layer are much smaller compared to the movements normal to the wall.

The use of these assumptions, permits the equations for continuity of mass and energy to be written as follows:

$$\frac{\partial \rho}{\partial t} + \frac{\partial (\rho u)}{\partial x} = 0 \qquad (21)$$

$$\rho C_p \frac{\partial T}{\partial t} + \rho C_p u \frac{\partial T}{\partial x} = \frac{DP}{Dt} + \frac{\partial}{\partial x}\left(\lambda \frac{\partial T}{\partial x}\right) + \rho \frac{dq}{dt} \qquad (22)$$

where u is the x component of the velocity and q is the volumetric rate of heat generation.

It is shown by Kumar (9) that the above system of equations can be reduced to the following equation.

$$\frac{\partial U}{\partial \sigma} = \alpha_o \frac{\partial^2 U}{\partial z^2} \qquad (23)$$

$$\text{where } \sigma = \int_o^t \frac{P}{P_o}\, dt \;, \quad z = \int_o^x \frac{\rho}{\rho_o}\, dx$$

$$\text{and } U = \frac{T}{T_\infty}$$

and α_o is the thermal diffusivity and T_∞ is the ambient gas temperature. The equation (23) can be described in non-dimensional form as follows

$$\frac{\partial U}{\partial s} = \frac{\partial^2 U}{\partial y^2} \qquad (24)$$

$$\text{where } s = \frac{\alpha_o}{\delta^2} \int_o^t \frac{P}{P_o}\, dt \qquad y = \frac{1}{\delta} \int_o^x \frac{\rho}{\rho_o}\, dx$$

and δ is the boundary layer thickness.

The boundary conditions are

$$U(y,o) = 1$$
$$U(o,s) = T_w/T_\infty \qquad (25)$$
$$U(\delta,s) = 1$$

Equation (24) is solved using an explicit finite difference technique with non-linear grid spacing. However, solution of (24) gives U as a function of s and y. In order to evaluate T(x,t), we need to make use of the following relations

$$s = \frac{\alpha_o \sigma}{\delta^2} \quad \text{and} \quad y = \frac{z}{\delta} \qquad (26)$$

Thus we need to know the pressure-time history in order to get the temperature profile in the boundary layer.

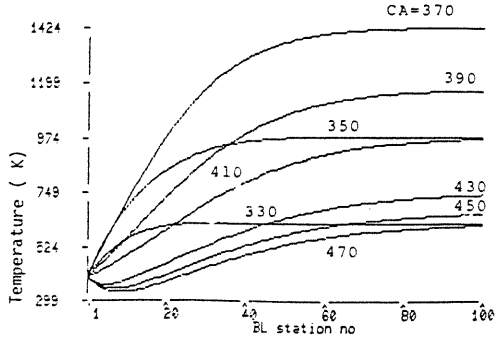

Fig. 2 Boundary layer temperature profiles at 20°CA increments during a non-firing compression and expansion

Figure (2) shows a typical boundary layer temperature profile obtained from the heat transfer model. Once the temperature profile is known, the wall heat flux $\dot{q}_w$ can be calculated as follows:

$$\dot{q}_w = -\lambda_w \left(\frac{\partial T}{\partial x}\right)_{x=o} \qquad (27)$$

Noteworthy are the results, late in the expansion process at 430,450 and 470 crank angle degrees. Heat flux from the wall to the gas is predicted when the gas temperature is greater than the wall temperature. This is in accord with our findings based on heat release analysis computed from cylinder pressure diagrams and as found in earlier work (13).

Overall Energy Conservation

The following energy exchanges are identified in the zones within the engine:

1. Jet zones:
   * Mass transfer into the zones.
   * Heat absorption as the result of droplet evaporation.
   * Heat release from fuel burning.
   * Heat transfer to the cylinder walls.
2. Air zone:
   * Heat transfer to the cylinder walls.
   * Mass transfer to the jet zones.

With the simplifying assumptions of constant pressure throughout the chamber, and complete mixing within zones but ignoring interzonal transfers, the energy equation for the zone is

$$\frac{d}{dt}(M_i U_i) = \frac{dM_b}{dt} \Delta H_R + \dot{Q}_{ev} + \dot{Q}_w + h_a \dot{M}_{a_i} + \dot{PV}_i \qquad (28)$$

where ΔH_R is the reaction enthalpy, Q_{ev} is the evaporation enthalpy derived from equation (16), Q_w is the wall heat transfer, h_a is the enthalpy of the entrained air, M_{a_i} is the rate of air entrainment, P is the cylinder pressure and V_i is the rate of volume change.

From the internal energy definition for the zone

$$\dot{U}_i = C_{v_i}\dot{T}_i \qquad (29)$$

$$\text{where } C_{v_i} = C_{v_i}(T_i, P, \phi_i)$$

Pressure and temperature are related through the equation of state

$$PV_i = M_i R_i T_i \qquad (30)$$

$$\text{where} \quad R_i = R_i(T_i, P, \phi_i)$$

Now the change in volume of the zones

$$\dot{V} = \sum \dot{V}_i \qquad (31)$$

where from Engine geometry:

$$\dot{V} = \frac{d}{dt}\left(V_{cl} + \pi\frac{d^2}{4}\left\{L_r + \frac{S_r}{2}(1-\cos\theta) - \left(L_r^2 - \frac{S_r^2}{4}\sin^2\theta\right)^{1/2}\right\}\right) \qquad (32)$$

where V_{cl} is clearance volume, d is cylinder bore, L_r is connecting rod length allowing for deflection due to mechanical load, S_r is the stroke and θ is the crank angle with respect to the top dead centre. The above set of equations can be simplified to the following form (9)

$$\dot{P} = (A_q - \dot{PV})/B_v \qquad (33)$$

$$\text{where} \quad A_q = \Sigma\frac{\dot{Q}_i + h_a\dot{M}_{a_i}}{(1+X_i)}$$

$$B_v = \Sigma\frac{V_i}{1+\frac{1}{X_i}} \quad \text{and} \quad X_i = C_{v_i}/R_i$$

Also for the individual zones we have the following,

$$\dot{V}_i = \frac{1}{P}\frac{\dot{Q}_i + h_a\dot{M}_{a_i}}{(1+X_i)} - \frac{\dot{P}}{P}\frac{V_i}{1+\frac{1}{X_i}} \qquad (34)$$

SOLUTION OF THE EQUATIONS

Code has been written in Pascal to solve the above set of equations numerically. It was found that with 0.02^o crank angle increments, a time step independent solution was obtained. The code is written with two modes of operation:

Diagnostic. In this mode it is assumed that all the calibration steps (droplet sizing, spray angle, jet penetration and fuel properties measurement have been performed, and describe the in cylinder process accurately. The effective values of K and E (the reaction kinetic coefficients) are determined as follows:

1. K and E are assumed from best estimates available.
2. The program at each time increment adjusts the values of τ uniformly for all reaction zones so that the predicted and measured cylinder pressures agree. The necessary variations of τ are stored in the data space of the variables P_i, ϕ_i and T_i in each zone. Best fit values of K and E are determined which minimises the error in the data space. These values are used in a repeat process and iteration continued until stable values of E and K are obtained.

Predictive. In the predictive mode the values of the fuels' physical and chemical properties follow the prescribed behaviour during the prediction of the in-cylinder process. This mode of operation is employed for validation and sensitivity analyses.

RESULTS

A Petter PH1W four stroke direct injection diesel engine was instrumented to record cylinder pressure, crank angle, piston position close to top centre and as indicated in fig 1 fuel injector needle lift and delivery pressure. The layout is shown schematically in fig. 3. Special attention has been paid to cylinder pressure and volume measurement since these are key input parameters in the diagnostic calculations. For example deflections in the connecting rod are known to cause cylinder volume increases corresponding to nearly one compression ratio at top centre. Hence the measurement of piston position and heat shielding of the pressure transducer.

Operation on Diesel Fuel

The matrix of diesel engine operation is given in table 1

Table 1.
Engine operating points

	Speed (r/min)		
	1250	1500	1700
	Full	Full	Full
Brake load	1250 Mid	1500 Mid	1700 Mid
	1250	1500	1700
	No	No	No

In addition to the constants previously assigned values for fuel spray penetration, spray angle and droplet size distribution coefficients were determined from the single shot, high pressure chamber tests.

Fig. 4 shows the penetration of the fuel jet as recorded by high speed photography at 3 operating pressures, seen in fig. 4 for full load conditions. The experiment was repeated for the two other fuel rack positions identified in Table 1.

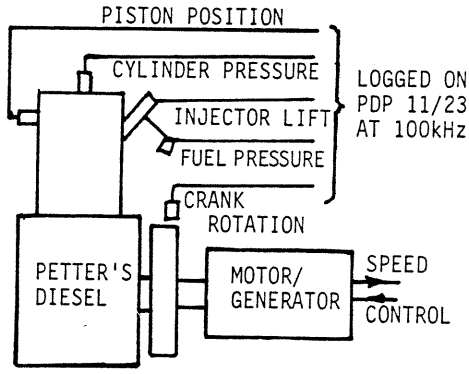

Fig. 3 Schematic of engine data acquisition

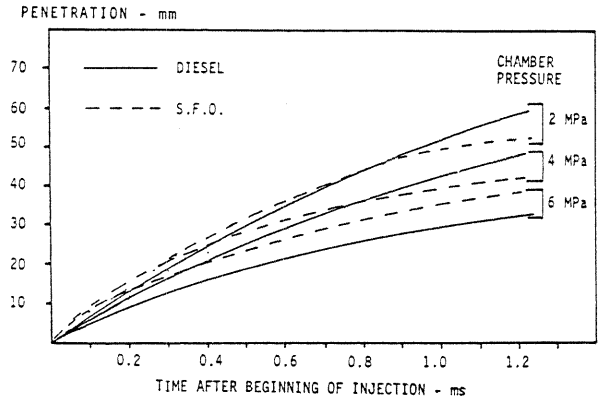

Fig. 4 Spray penetration vs time from the start of injection for diesel and S.F.O. at full load rack setting under a range of chamber pressures.

Examination of the slope of penetration curves in fig. 4 indicates the higher initial jet velocity of sunflower oil (S.F.O.) compared with diesel oil, but less overall penetration at each of the 3 chamber pressures.

From these data and those at the other loads it was determined (13) that in equation 8 the coefficient was

C_1 = 1.081 for diesel oil
C_1 = 0.899 for S.F.O.

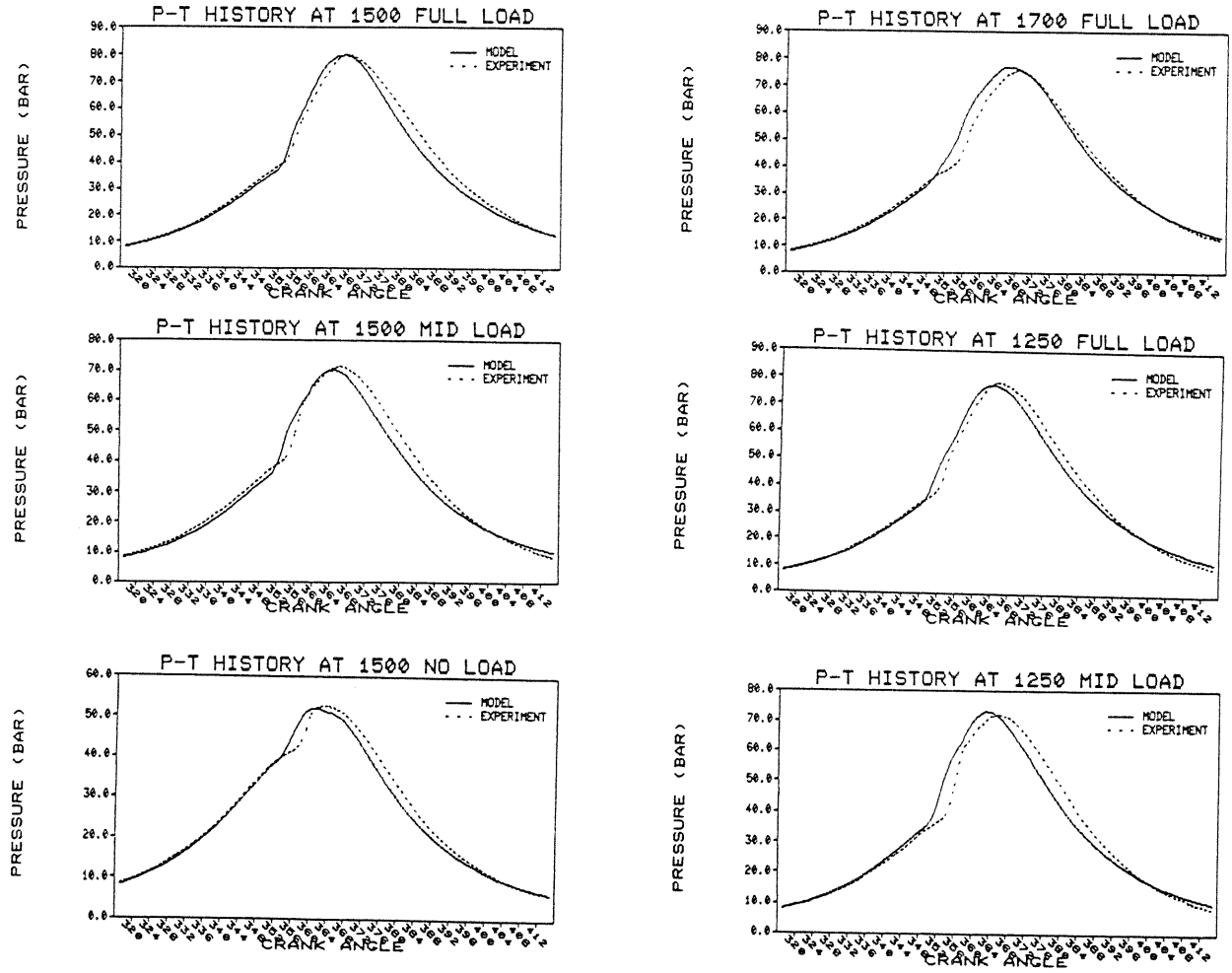

Fig. 5 Measured and predicted cylinder pressure-time histories for three loads and speeds using diesel fuel

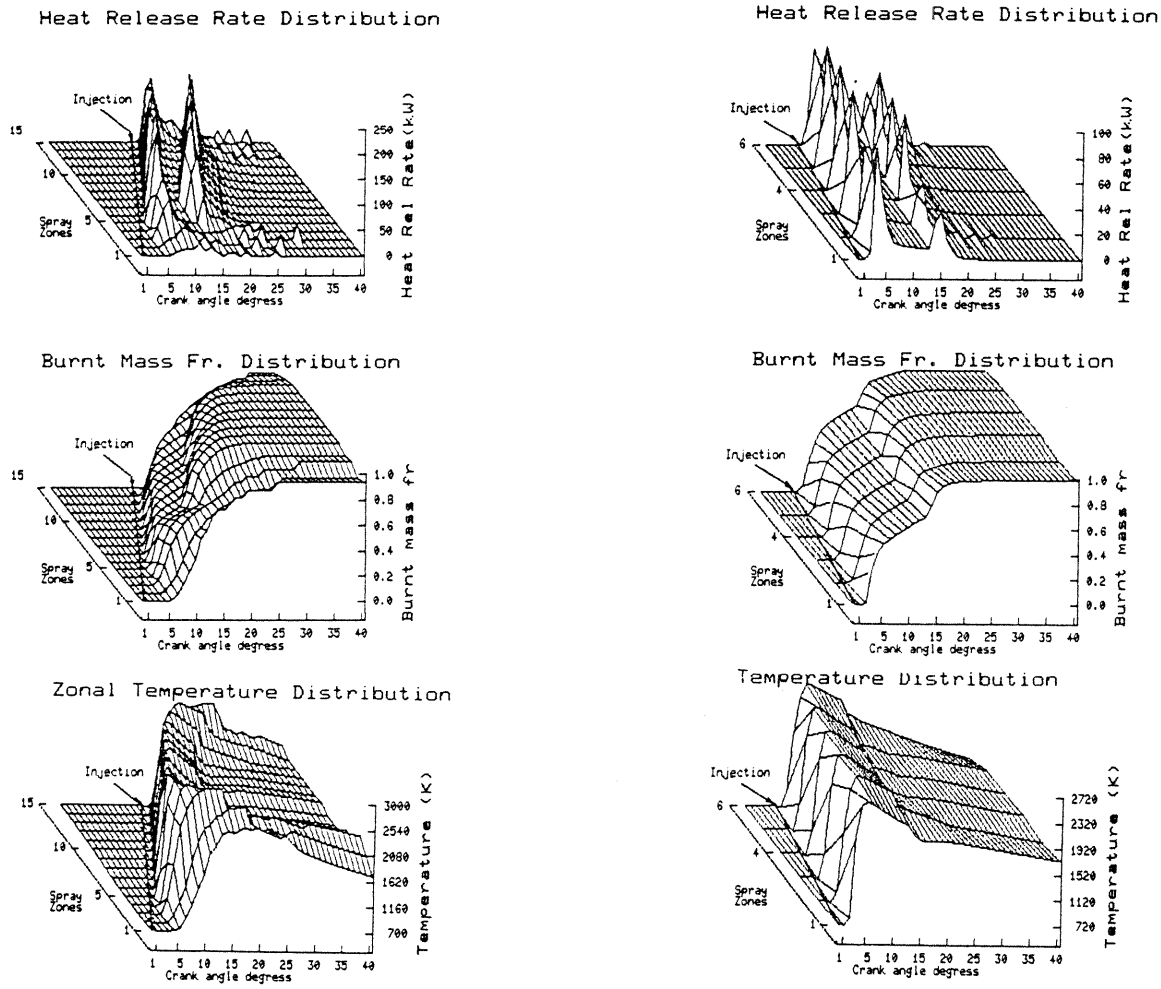

Fig. 6 Heat release rate, burnt mass fraction and temperature surfaces for full and no loads at 1500 r/min engine speed on diesel fuel

for the 1500 r/min operating speed. The corresponding mean spray angles were measured (14)

Diesel Fuel Predictions

Use of the above data enabled the prediction of cylinder pressures seen in fig. 5. Results for all 3 loads at 1500 r/min on the left side show close agreement with experimental measurement. The right side shows corresponding diagrams at full load at 1700 r/min and full and half loads at 1250 r/min.

More details from the simulation are presented in fig. 6 for the 1500 r/min full and no load cases. The heat release rate diagram depicts qualitatively the expected results. The first injected fuel zone experiences a 6° delay before combustion begins. Indeed it is zone 3 which because of higher velocity and faster fuel evaporation burns first. Zone numbers greater than 5 experience very little delay consistent with the concept of diffusion burning. Because there is insufficient entrainment of air into the spray zones, it is only when the zones impinge on the wall that the increased entrainment of the wall jet allows combustion completion and gives rise to the second series of peaks (or ridge) in heat release rate. The corresponding increases in burnt mass fraction can be viewed in the middle figures.

The first and last injected zones are seen to burn most slowly and have lowest temperatures in the bottom graphs.

The role of the wall-jet in completing combustion is not inconsistent with the nature of the combustion chamber bowl deposits opposite each of the 3 injector holes, which exhibit dark soot formations where the core of the jet impinges on the wall, and lighter deposits away from the core of the jet where velocities are expected to be greater.

Sun Flower Oil

Our work on the analysis of the performance of S.F.O. is at a preliminary stage. The evaluation of the effective rate constants for the S.F.O. oxidation process is not complete. However fig. 7 demonstrates our ability to predict the indicator diagram for S.F.O. combustion. Plainly some refinement is needed before S.F.O. performance prediction is of the same quality as that for diesel oil.

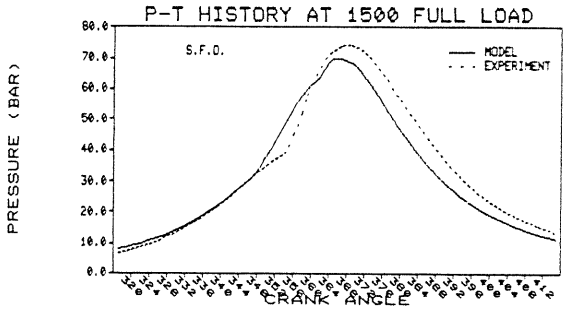

Fig. 7 Predicted pressure-time history for S.F.O.

CONCLUSIONS

The model presented describes the phenomena of fuel injection, fuel jet penetration, droplet formation and evaporation fuel-air mixing and burning for the open chamber diesel engine. The first 3 stages of the model have been calibrated outside the engine with the aid of a high pressure chamber containing nitrogen so that optical measurements of the fuel jet could be made.

When employed in its diagnostic mode of operation the model permits the estimation of the fuel oxidation relaxation parameter τ, which can later be related to the overall reaction rate constants in the Arrhenuis reaction rate expression.

Previously estimated values of rate constants for diesel fuel oxidation (11) already appear to give good estimation of the combustion process over a wide range of engine operation when the model is employed in the predictive mode. Cylinder pressure diagrams are shown to agree closely with experimental measurements in Fig. 5.

Determination of the model coefficients for the plant oils is at a preliminary stage. However, already it has been shown that the penetration rate of sunflower oil is greater than that of diesel oil and the spray angles are narrower.

Since the growth of the wall jet following impingement on the combustion chamber bowl wall is predicted to provide extra air entrainment which helps combustion completion, more wall interaction in the case of sunflower oil may contribute to deposit formation and hence ring sticking. Confirmation of this hypothesis should be available when the esters of sunflower oil have been tested.

REFERENCES

1. Ryan III, T.W., Callahan, T.J., Dodge, L.G., and Moses, C.A., "Development of a Preliminary Specification for Vegetable Oil Fuels for Diesel Engines," Final Technical Report No. SWRI-6753 South West Research Institute, San Antonio, Texas, U.S.A., April 1983.

2. Quick, G.R., Wilson, B.T., and Woodmore, P.J.,"Injector Fouling Propensity of Certain Vegetable Oils and Derivatives as Fuels for Diesel Engines," Proceedings of the Inernational Conference on Plant and Vegetable Oils as Fuels, pp 239-246, American Society of Agricultural Engineers, August 1982.

3. Wylie, E.B., Bolt, J.A., and El-Erian, M.F., "Diesel Fuel Injection System Simulation and Experimental Correlation," S.A.E. Paper 710569, 1971.

4. Kumar, S., "Thesis in Preparation," University of Melbourne.

5. Hiroyasu, H. and Kadota, T., "Models for Combustion and Formation of Nitric Oxide and Soot in Direct Injection Diesel Engines," S.A.E. Trans., Vol. 85, Paper No. 760129, 1976.

6. Hiraki, H., and Rife, J.M., "Performance and NO_x Model of a Direct Injection Stratified Charge Engine," S.A.E. Trans., Vol. 89, Paper No. 800050, 1980.

7. Kamimoto, T. and Matsouka, S., "Prediction of Spray Evaporation in Reciprocating Engines," S.A.E. Paper No. 770413, 1977.

8. Hiroyasu, H., Kadota, T. and Arai, M., Supplementary Comments: "Fuel Spray Characterization in Diesel Engines," Combustion Modeling in Reciprocating Engines edited by Mattavi, J.N., and Amann, C.A., Plenum Press, New York, 1980

9. Kumar, S., "A Model for the Analysis and Prediction of Heat and Mass Transfer and Combustion of Fuels in Diesel Engines," Report T65/84, Department of Mechanical Engineering, University of Melbourne, July 1984.

10. Zeleznik, F.J., "Combustion Modeling in Internal Combustion Engines," Combustion Science and Technology, Vol. 12, pp. 159-164, 1976.

11. Parker, T.E., Forsha, M.D., Stewart, H.E., Hom, K., Sawyer, R.F., and Oppenheim, A.K., "Induction Period for Ignition of Fuel Sprays at High Temperatures and Pressures," S.A.E. Paper 850087, 1985.

12. Chong, M.S., Milkins, E.E. and Watson, H.C., "The Prediction of Heat and Mass Transfer during Compression and Expansion in I.C. Engines," S.A.E. Trans., Vol. 84, Paper No. 760761, 1976.

13. Milkins, E.E., "Heat Transfer in a Rapidly Compressed Gas," M.Sc.(Eng.) thesis, Imperial College of Science and Technology, London, 1967.

14. Edsell, J., "Comparison of Injected Behavior of Diesel and Plant Oils using High Speed Photography," Technical Report T66/84, Department of Mechanical and Industrial Engineering, University of Melbourne, Australia, 1984.

15. Poreh, M., Tsuei, Y.G., and Cermak, J.E., "Investigation of a Turbulent Radial Wall Jet," Journal of Applied Mechanics, Vol. 34, pp. 457-463, 1967.

ACKNOWLEDGEMENT

The funding for this project from the National Energy Research Development and Demonstration Council of the Department of Resources and Energy is gratefully acknowledged. The co-operation of the C.S.I.R.O. Division of Energy Technology and The Repco Engine Technical Centre in assisting in the high pressure test chamber studies of fuel injection made a significant contribution to the project.

APPENDIX A

HIGH PRESSURE TEST CHAMBER

A high pressure test chamber was built to study the performance of the engine fuel injector and fuel jet development. The plane cylindrical chamber is of similar dimensions to the combustion chamber in the engine. The cylinder is 48 mm long and 90 mm diameter with its ends closed by 25 mm thick clear acrylic windows. However, the fuel injector is located in periphery of the chamber in such a way that one nozzle fired diametrically across the chamber, whilst the two remaining nozzles discharge around the wall of the chamber. Thus the penetration of the central jet is 90 mm prior to wall impingement compared to only 25 mm in the engine. The maximum gas working pressure was designed at 8 MPa.

The same fuel pump as used on the engine is operated by a single shot mechanism consisting of a pneumatically driven ram driving a cam through a rack and pinion. The cam profile gives the same lift-time diagram as the engine camshaft and speeds up to 1700 r/min equivalent.

The apparatus was used for the measurement of jet penetration, jet spray angle and droplet size distribution. The first two measurements being performed at 5700 frames/s using a 'Hycam I' camera and high speed black and white film. Droplet sizing is achieved with the use of Malvern Model 2600/3600 laser droplet sizer, specially modified to allow sampling intervals of down to 0.5 ms.

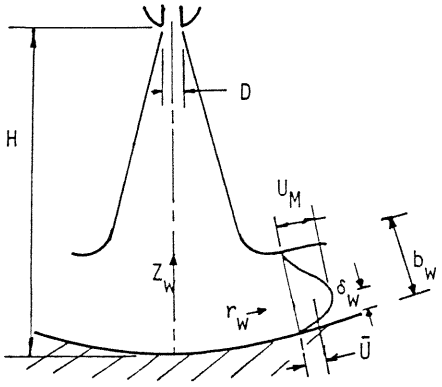

Fig. 8 Diagram of symbols meaning used in wall jet analysis.

APPENDIX B

DESCRIPTION OF WALL JET

Figure 8 shows the schematic description of the wall jet impingement.

The dimensionless velocity distribution in the radial wall jet produced by an impinging circular jet is described by Poreh et al (15). The velocity distribution data was fitted to the following equation

$$\frac{U_z}{U_M} = C_5\{1-\frac{Z_w}{\delta_w}\} + C_6\{\frac{Z_w}{\delta_w}\} + C_7\{1-(\frac{Z_w}{\delta_w})^3\} + C_8 \ln\{\frac{Z_w}{\delta_w}\} \quad (B1)$$

where U_z is the velocity at Z_w and U_M is the maximum velocity. δ_w is defined as follows

$$(U_z)_{\delta_w} = \frac{1}{2} U_M \quad (B2)$$

C_5, C_6, C_7 and C_8 are constants and their values are found to be as follows

$$C_5 = 1.716$$
$$C_6 = 0.466$$
$$C_7 = -0.728$$
$$C_8 = 0.09$$

Now from mass conservation,

$$\dot{m}_w = 2\pi\rho_e b_w \int_0^{b_w} U_z \, dZ_w \quad (B3)$$

where b_w is the width of the jet and ρ_e is the density of flow.

For wall jet, the following equations describe U_M and δ_w

$$\frac{U_M r_w}{\sqrt{K_m}} = 1.32 \left(\frac{r_w}{H}\right)^{-0.1} \quad (B4)$$

$$\frac{\delta_w}{r_w} = 0.098 \left(\frac{r_w}{b_w}\right)^{-0.1} \quad (B5)$$

where K_M is the kinematic momentum flux at nozzle exist and H is the distance between wall and nozzle exit.
If we assume that $b_w = 3\delta_w$ then it can be shown that

$$\frac{\dot{m}_w}{r_w(\rho_e(\dot{m}_i)_o u_o)^{1/2}} = 8.32\left(\frac{r_w}{H}\right)^{-0.3} \quad (B6)$$

Rearrangement of equation (B6) gives the following equation which describes the air-entrainment in the wall jet.

$$\frac{\dot{m}_w}{(\dot{m}_i)_o} = 9.386 \left(\frac{r_w}{D}\right) \left(\frac{r_w}{H}\right)^{-0.3} \quad (B7)$$

Now, we know that

$$\frac{dr_w}{dt} = \bar{U}_w \qquad (B8)$$

where U_w is the mean velocity at r_w

Equation (B8) is integrated to arrive at the following equation for wall jet penetration.

$$r_w = C_2 (u_0 D t_w H^{0.2})^{1/2.2} \qquad (B9)$$

where t_w is the time from commencement of wall jet.

NOMENCLATURE

A = area (m^2)
A_q = regrouped variable
B^q = amount of fuel delivered (m^3/stroke)
B_v = regrouped variable
b = burnt mass fraction
b_w = width of wall jet (m)
C = flow resistance (m^2)
C_d = droplet drag coefficient
C_p = specific heat at constant pressure (J/kgK)
C_v = specific heat at constant volume (J/kg K)
D = nozzle diameter (m)
D_d = droplet diameter (m)
D_s = Sauter mean diameter (m)
D_v = diffusion coefficient (m^2/s)
E = activation energy (J/kg)
H = distance of nozzle tip from combustion bowl (m)
h = enthalpy (J/kg)
ΔH_R = enthalpy of reaction (J/kg)
K = pre-exponential constant
K_m = kinematic momentum flux (m^4/s^2)
k = coefficient of compressibility (N/m^2)
L_r = connecting rod length (m)
M = gaseous mass (kg)
m = fuel mass (kg)
N = fuel injector cam speed (r/min)
Nu = Nusselt number
P = pressure (N/m^2)
ΔP = pressure differnce between injector tip and combustion chamber (N/m^2)
Q = volumetric flow (m3/s),
= heat transfer (J)
Q_d = volumetric discharge from nozzle (m^3/s)
$\dot{q}$ = volumetric rate of heat generation (W/m^3)
R = gas constant (J/kg K)
r = radial penetration (m)
S = needle lift (m)
Sh = Sherwood number
S_p = axial penetration (m)
S_r = stroke (m)
s = transformed coordinate
t = time (s)
T = temperature (K)
U = internal energy (J/kg K)
= wall jet velocity (m/s)
u = transformed coordinate
V = volume (m^3)
v = velocity (m/s)
X = regrouped variable
x = x coordinate
y = transformed coordinate
Z_w = axial distance from combustion bowl (m)
z = transformed coordinate

α = semi-spray angle (degrees)
α_o = diffusivity at standard conditions (m^2/s)
ψ = regrouped variable
ϕ = fuel air equivalence ratio
λ = thermal conductivity (W/m K)
ρ = density (kg/m^3)
θ = crank angle with respect to TDC (degrees)
σ = transformed variable
τ = relaxation coefficient
δ = boundary layer thickness (m)
δ_w = distance at which the wall jet velocity is half of maximum (m)

Subscripts
a = air
b = burnt mass
c = chamber volume upstream of injector needle seat
cl = clearance volume
d = droplet
e = entrained
ev = evaporation
f = fuel
fg = vaporisation
fv = fuel vapor
fvs = fuel vapor saturated
i = zone i
j = step j
L = line
M = maximum
s = sac volume
u = upper nozzle chamber
w = wall
z = z coordinate
∞ = ambient